Article

Multi-Electron Ionization and Coulomb Explosion of the IBr Molecule in the Near-Infrared Femtosecond Laser Field

Botong Liu [1], Zhipeng Li [2], Zhenrong Sun [2] and Yan Yang [2],*

1   School of Information Engineering, Yancheng Institute of Technology, Yancheng 224051, China; liubot@ycit.edu.cn

2   State Key Laboratory of Precision Spectroscopy, School of Physics and Electronic Science, East China Normal University, Shanghai 200062, China; 15201715520@163.com (Z.L.); zrsun@phy.ecnu.edu.cn (Z.S.)

*   Correspondence: yyang@lps.ecnu.edu.cn

Abstract: The DC-sliced ion velocity map imaging approach was used to analyze the multi-electron ionization and subsequent Coulomb explosion of an IBr molecule exposed to a near-infrared femtosecond laser field. The existence of the molecular ions up to IBr^{7+} was observed in the experiment, and a series of Coulomb explosion channels are assigned. According to the "ladder-path" ionization model, the multi-electron ionization paths of IBr molecules are determined. We find that the charge transfer process does not occur during ionization, and the presence of higher charge states can be explained by considering the higher-order ionization process.

Keywords: multi-electron ionization; Coulomb explosion; femtosecond laser field

1. Introduction

Ionization is one of the most fundamental physical processes in the interaction between intense lasers and matter. The ionization process governs many other physical processes, including high harmonic generation, photoelectron holographic imaging, molecular dissociation, electron correlation, etc. [1–9]. With the development of femtosecond and attosecond laser pulses, scientists now have better knowledge of ionization [10–18]. The Keldysh parameter value can be utilized to identify the ionization process under various laser conditions [19,20]. When the Keldysh parameter exceeds one, an electron can absorb multiple photons simultaneously and overcome the ionization potential. When the Keldysh parameter is far less than one, the laser field instead significantly suppresses the Coulomb potential, and electrons escape through tunneling across the potential energy surface.

Recently, there has been significant interest in multi-electron ionization in a strong laser field. To understand the dynamic processes involved, a variety of theoretical models have been developed. The femtosecond laser field may swiftly remove many electrons with minimum change to the molecule structure. Next, the Coulomb repulsive force affects the charged molecular ions' dissociation, according to the multi-electron dissociative ionization (MEDI) model [21]. In the post-dissociative ionization (PDI) model, reaction products may undergo a second ionization process after dissociation [22]. Conversely, the two-step model proposes that molecule electron loss and, at equilibrium and critical distances, Coulomb explosions (CE) occur twice [23]. Bandrauk et al. put forward a model of charge resonance enhanced ionization (CREI), wherein they showcased the charge resonant states, highlighting a strong correlation with the laser field at a given distance R_c [24]. Based on this model, all charged molecular ions exhibit an identical energy defect ratio. However, Gibson et al. proposed a sequential ionization process for CREI, whereby the electrons are stripped one by one in a laser pulse and nuclear stretching cannot be averted [25]. The energy collected in the previous ionization step is also included in the kinetic energy (KE) that accumulates from each channel. As a result, rather than having a constant value, the R_c value should fluctuate when the charge states change [26]. Thus, it is important

to investigate what causes these dissociation processes, as well as how kinetic energy accumulates in the molecules before dissociation.

Most studies are mostly focused on homo-nuclear halogen molecules, such as H_2, N_2 and I_2 [26–31]. The study of the dissociation and ionization process for heteronuclear halogen molecules has been relatively underreported. As a classical heteronuclear halogen molecule, IBr has mostly been studied for the coherent control of the photo-dissociation process [32–35]. However, we are interested in the intense field dynamic process of IBr. In this paper, we explore the ultrafast dynamics processes of multi-electron ionization and the Coulomb explosion (CE) of IBr in the near-infrared femtosecond laser field. Our results show that high-charged molecular ions are formed when electron ionization is enhanced by increasing nuclear separation. Furthermore, the charge transfer process does not occur in the process and higher-order ionization processes need be considered to achieve higher charge states. This work can provide an understanding of the complex field-induced multi-electron dynamics of heteronuclear diatomic molecules.

2. Experiment and Theory Calculation

An in-house DC-sliced velocity imaging system was utilized to carry out the experiment. The system has been further detailed elsewhere [36,37]. In brief, a biconvex lens focuses femtosecond laser pulses into the reaction chamber at a repetition rate of 1 kHz, a center wavelength of 800 nm, and a pulse duration of 70 fs. The polarization vector of the laser is perpendicular to the direction of ion flight, and the laser intensity in the focal volume is estimated to be 40 to 300 TW/cm^2, which was calibrated by measuring the yield ratio of Ar^{2+}/Ar^+ [38]. After being seeded with helium in a 1:10 ratio, the gaseous iodine bromide sample is expelled into the reaction chamber (~5.0×10^{-9} mbar) using a pulsed valve (General Valve, Parker, Cleveland, OH, USA) that repeats at a rate of 100 Hz for 130 μs. The supersonic molecular beam interacts at a right angle with the linearly polarized femtosecond pulse in the middle of the extraction and repeller plates. As the fragment ion clouds pass through the velocity mapping lens, they are stretched and detected using micro-channel plates (MCPs) coupled with the P47 phosphor screen. An oscilloscope (LeCroy Wave Pro) is coupled to a photomultiplier tube (Hamamatsu H7732-11), which records the related time-of-flight (TOF) mass spectra in one dimension. An intensified charge-coupled device camera (ICCD, PI-MAXII) with a time resolution of 5 ns is used to capture the two-dimensional images. Utilizing a digital delay/pulse generator (DG645, Stanford Instruments, Sunnyvale, CA, USA), timing sequencing control is performed.

To enhance the comprehension of the ultrafast dynamic processes involved in the IBr molecule, we conducted various theoretical calculations by using the Gaussian 09 software [39]. The molecular structure was optimized using the B3LYP/aug-cc-pVTZ level [40,41]. The potential energy curves of ionic IBr^{2+} were calculated at the EOM-CCSD level of theory using a def2TZVP basis set [42,43].

3. Results

Figure 1a–c show the TOF mass spectra of an IBr molecule exposed to an 800 nm femtosecond laser pulse with a pulse duration of 70 femtoseconds (FWHM). The laser intensities are (a) 40 TW/cm^2, (b) 90 TW/cm^2, and (c) 300 TW/cm^2, respectively. In our work, dissociative ionization dominates the dissociation and ionization process due to the femtosecond laser field. A series of ions, Br^{m+} (m = 1–3) and I^{n+} (n = 1–4), are observed, implying that the parent molecule ions are highly unstable and easily break down into fragment ions. At a low laser intensity, the ions Br^+, I^+, and I^{2+} are the main products. As the laser intensity increases, the generation of multipe-charged ions Br^{m+} (m = 2–3) and I^{n+} (n = 3–4) shows the involvement of Coulomb explosion processes (CE) in this experiment. In addition, the raw DC-sliced ion images (512 × 512 pixel) and the normalized velocity distributions of the ions I^{n+} (n = 1–4) and Br^{m+} (m = 1–3) are shown in Figure 2.
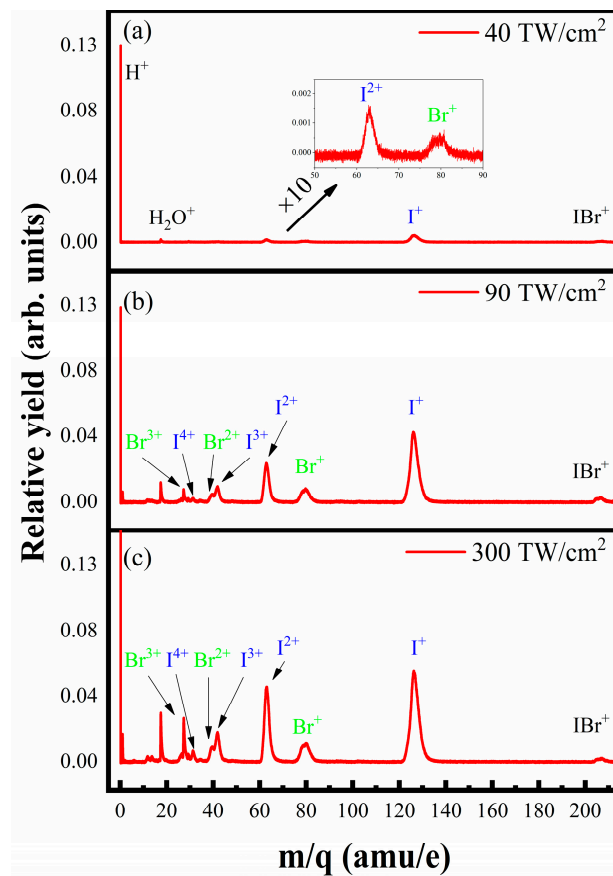
Figure 1. TOF mass spectra of the molecule IBr at (**a**) 40 TW/cm², (**b**) 90 TW/cm², and (**c**) 300 TW/cm², respectively.
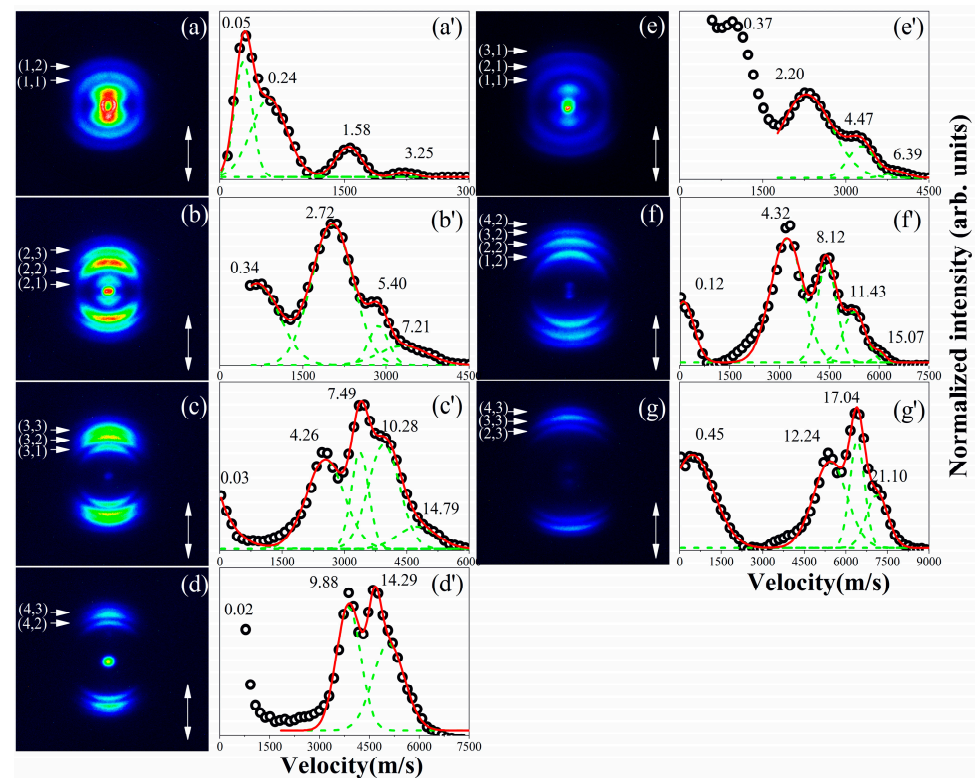

Figure 2. The raw DC-sliced images (512 × 512 pixel) of the fragment ions (**a**) I⁺, (**b**) I²⁺, (**c**) I³⁺, (**d**) I⁴⁺, (**e**) Br⁺, (**f**) Br²⁺, and (**g**) Br³⁺ at the intensity of 300 TW/cm². The laser polarization direction

is represented by the double-headed arrow. The estimated dissociation process, $IBr^{(n+m)+} \rightarrow I^{n+} + Br^{m+}$, is represented by the channel (p, q). The corresponding velocity distributions of the fragment ions (**a'**) I^+, (**b'**) I^{2+}, (**c'**) I^{3+}, (**d'**) I^{4+}, (**e'**) Br^+, (**f'**) Br^{2+}, and (**g'**) Br^{3+} are also shown, in which the intensities have been normalized. The KER in eV is labeled in (**a'–g'**). The experimental data are represented by the circles, while the fitting peaks are represented by the green dashed lines and the sum of the fitting peaks are presented by the red solid lines.

4. Discussion

As shown in the polycyclic structure of Figure 2a–g, it is clear that fragment ions with the same charge state come from different reaction channels. The corresponding KER values have been extracted and labeled in Figure 2a'–g'. It can be seen that all these ion kinetic energy distributions have both high and low kinetic energy components. Generally, the multiphoton dissociative ionization (MPDI) process would produce fragment ions with low KER (<0.5 eV), while the Coulomb explosion (CE) process would produce fragment ions with high KER [44]. Here, we concentrate on these channels in the CE processes.

$$KER(A^{P+})/KER(B^{q+}) = M(B^{q+})/M(A^{P+}), \tag{1}$$

$$KER\_total = 14.4pq/r, \tag{2}$$

In the classical two-body CE model, two fragmented ions should satisfy momentum conservation, as explained by Equation (1), where A^{P+} and B^{q+} represent the two fragment ions, p/q denote the charge states, and M stand for the mass of the fragment ions. Equation (2) represents the total KER of a CE channel, where r indicates the internuclear distance when the CE starts. Based on the equations given above, the possible CE channels are listed in Table 1.

Table 1. The possible CE channels for the molecular ions IBr^{x+} (x = 2–7).

(n, m)	CE Channels	KER_I^{n+} (eV)	KER_B^{m+} (eV)	KER_total (eV)	R_c (Å)
(1, 1)	$IBr^{2+} \rightarrow I^+ + Br^+$	1.58	2.20	3.78	3.81
(1, 2)	$IBr^{3+} \rightarrow I^+ + Br^{2+}$	3.25	4.32	7.57	3.80
(2, 1)	$IBr^{3+} \rightarrow I^{2+} + Br^+$	2.72	4.47	7.19	4.01
(2, 2)	$IBr^{4+} \rightarrow I^{2+} + Br^{2+}$	5.40	8.12	13.52	4.26
(2, 3)	$IBr^{5+} \rightarrow I^{2+} + Br^{3+}$	7.21	12.24	19.45	4.44
(3, 1)	$IBr^{4+} \rightarrow I^{3+} + Br^+$	4.26	6.39	10.65	4.06
(3, 2)	$IBr^{5+} \rightarrow I^{3+} + Br^{2+}$	7.49	11.43	18.92	4.57
(3, 3)	$IBr^{6+} \rightarrow I^{3+} + Br^{3+}$	10.28	17.04	27.32	4.74
(4, 2)	$IBr^{6+} \rightarrow I^{4+} + Br^{2+}$	9.88	15.07	24.95	4.62
(4, 3)	$IBr^{7+} \rightarrow I^{4+} + Br^{3+}$	14.29	21.10	35.39	4.88

The channel (n, m) represents the predicted CE process, $IBr^{(n+m)+} \rightarrow I^{n+} + Br^{m+}$. The energy collected in the previous ionization step is included in the KER that accumulates from each channel, as seen by the R_c changing with the charge states in Table 1. It is generally believed that the time for the double ionization to occur is more than a dozen fs. On this time scale, the molecular structure (e.g., the distance between nuclei) does not change. Therefore, the starting point of multi-electron ionization or the site where the third electron is ionized should still be at the equilibrium internuclear distance (R_e = 2.47 Å). Next, some theoretical calculations are performed to verify the above assumptions.

Figure 3 shows the dissociation potential energy (PE) curves of the ground electronic state and excited states of IBr^{2+} ion where the PE curves of the ionic IBr^{2+} are calculated at the def2TZVP/EOM-CCSD level and the pink rectangles show the ±0.05 Å region around the R_e. The charge-repulsive (CP) curves, as described by Equation (2), are also included. Similar to the relationship shown in ref. [45], the PE curve and CP curve will overlap when the nuclei are spread far apart enough. Here, we have defined E(∞) = 0 eV, so that the green line (3.78 eV) represents the measured KER of the channel (1, 1). If IBr^{2+} were to experience

a succeeding Coulomb explosion at R_e, the channel would be expected to release a total kinetic energy of 5.83 eV. However, the experimental result exhibits a much lower value, due to the fact that the chemical bond binding impacts the CE process of low-charge parent ions. As a result, a dissociation process taking place in the PE curves, as opposed to the CP curve, ought to make sense. In the pink rectangle area in Figure 3a,b, the PE curve coincides with the green line, which is in line with the experimental results. Thus, the starting point of multi-electron ionization is determined to be at R_e.
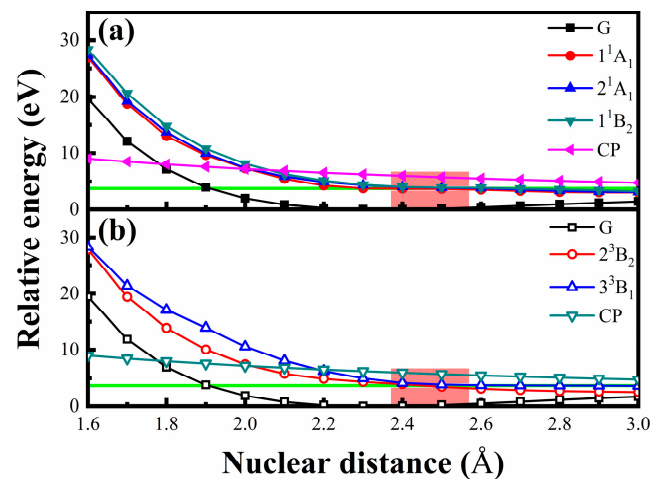

Figure 3. PE curves illustrating the IBr^{2+} ion's ground and excited states in the (**a**) singlet and (**b**) triplet states, respectively. The CP curve represents the relationship between Coulomb repulsion energy and nuclear distance. The pink rectangles show the ± 0.05 Å region around the Re and the green line represents the measured KER of the channel (1, 1).

Using the potential energy of the parent ions IBr^{x+} (x = 2–7), we calculated the critical distance, $R_{i,j}$. The relationship between the KER, $E_{i,j}$, and the potential energy V are described as follows [25,46]:

$$E_{n,m}^{exp} = V_{n,m}(R_{n,m}) - V(\infty), \tag{3}$$

where we define the V at infinity as zero. However, Equation (3) does not account for the accumulated kinetic energy recoveries from earlier stages. Consequently, it is necessary to include the accumulated KER:

$$E_{n,m}^{exp} V_{n,m}(R_{n,m}) + E_{n,m}^{acc}, \tag{4}$$

The accumulated KER can be written as follows:

$$E_{n,m}^{exp} - E_{i,j}^{exp} = V_{n,m}(R_{n,m}) + E_{n,m}^{acc} - V_{i,j}(R_{i,j}) - E_{i,j}^{acc}, \tag{5}$$

The energy increment accumulated between (i, j) and (n, m) can be expressed as follows:

$$\Delta E = E_{n,m}^{acc} - E_{i,j}^{acc} = V_{i,j}(R_{i,j}) - V_{i,j}(R_{n,m}), \tag{6}$$

Substituting Equation (6) into Equation (5), we arrived at:

$$E_{n,m}^{exp} - E_{i,j}^{exp} = V_{n,m}(R_{n,m}) - V_{i,j}(R_{n,m}), \tag{7}$$

Chemical bonding interactions between two atoms are significant at shorter nuclear distances, but they become negligible when the distance exceeds 3 Å. At this point, the Coulomb

repulsive force of two positive charges dominates the interaction process. $V_{n,m}(R_{n,m})$ can be expressed as Equation (2), and Equation (7) can be expressed to Equation (8).

$$E_{n,m}^{exp} - E_{i,j}^{exp} = 14.4 \text{ nm}/R_{n,m} - 14.4ij/R_{n,m} = 14.4(nm - ij)/R_{n,m} \tag{8}$$

Once both $V_{n,m}(R_{n,m})$ and $R_{n,m}$ are known, it becomes feasible to estimate the time needed to progress from one ionization stage to the next [25,47], as expressed by Equation (9).

$$T_{i,j \to n,m} = \int_{R_{i,j}}^{R_{n,m}} \frac{dr}{\sqrt{\frac{4}{m}[V_{i,j}(R_{i,j}) - V_{i,j}(r)]}}, \tag{9}$$

By substituting the measured KER values into Equations (8) and (9), we can obtain all possible critical distances and the corresponding travel times for each channel of one-electron sequential ionization, as shown in Table 2.

Table 2. The critical distance $R_{i,j}$ and the travel time, $T_{i,j \to n,m}$, for each channel of one-electron sequential ionization.

Process	Channel	$R_{i,j}$ (Å)	$T_{ij \to nm}$ (fs)
(a)	$(1, 1) \to (1, 2)$	3.80	17.55
	$(1, 2) \to (2, 2)$	4.84	16.25
	$(2, 2) \to (2, 3)$	4.86	7.28
	$(2, 3) \to (3, 3)$	5.49	9.13
	$(3, 3) \to (4, 3)$	5.35	/
(b)	$(1, 1) \to (1, 2)$	3.80	17.55
	$(1, 2) \to (2, 2)$	4.84	16.25
	$(2, 2) \to (3, 2)$	5.33	11.73
	$(3, 2) \to (3, 3)$	5.14	/
(c)	$(1, 1) \to (2, 1)$	4.22	20.55
	$(2, 1) \to (2, 2)$	4.55	9.86
	$(2, 2) \to (2, 3)$	4.86	7.28
	$(2, 3) \to (3, 3)$	5.49	9.13
	$(3, 3) \to (4, 3)$	5.35	/
(d)	$(1, 1) \to (2, 1)$	4.22	20.55
	$(2, 1) \to (2, 2)$	4.55	9.86
	$(2, 2) \to (3, 2)$	5.33	11.73
	$(3, 2) \to (3, 3)$	5.14	/
(e)	$(1, 1) \to (2, 1)$	4.22	20.55
	$(2, 1) \to (3, 1)$	4.16	/

Based on the experimental results, we can invert the one-electron sequential ionization process. Table 2 lists all the possible ionization paths. Based on the different Coulomb explosion channels, we can classify the above ionization paths into five categories, as shown in (a)–(e). It is noted that most of the $R_{n,m+1}$ or $R_{n+1,m}$ are larger than $R_{n,m}$, which is in line with the "ladder-path" model's prediction, but there are some ionization processes that are not reasonable. Taking process (a) as an example, IBr^{5+} ionized to IBr^{6+} at $R_{2,3} = 5.49$ Å, while IBr^{6+} further ionized to IBr^{7+} at $R_{3,3} = 5.35$ Å. The calculation result shows that $R_{n+1,m} < R_{n,m}$, which contradicts common sense. Naturally, it is also impossible to calculate the travel time according to Equation (9). The other processes (b)–(e) again fail to explain the existence of the experimental result of the channel (4, 3). Other experimental results, such as (3, 1) and (4, 2), present the same dilemma. Hence, we have considered two possible situations to explain the generation of these unreachable charge states; one involves the charge transfer (CT) process shown in Figure 4, while the other is the occurrence of the higher-order ionization process.
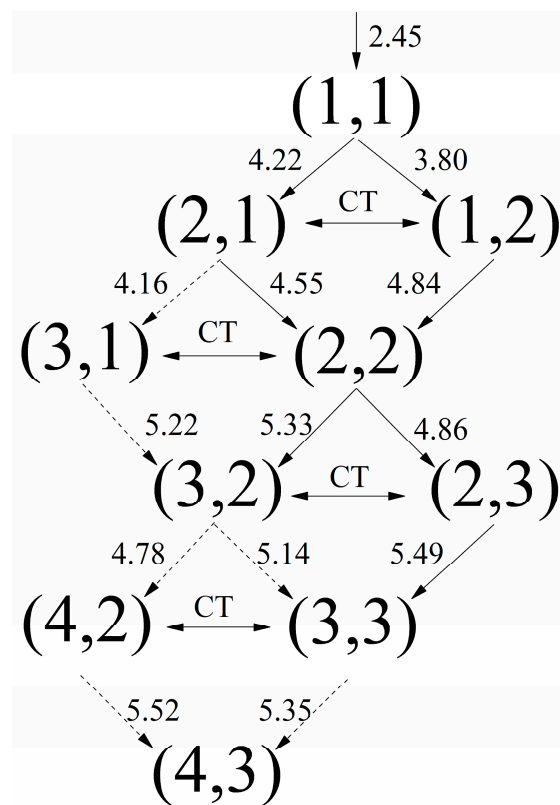
Figure 4. Molecular IBr's one-electron ionization pathways. The values situated above the arrow signify R (Å) during ionization. Charge transfer is represented by CT. Processes indicated by solid arrows are acceptable, whereas those indicated by dotted arrows are not.

First, we consider the effects of the existence of a CT process on the one-electron sequential ionization process. Here, the CT process is defined as $A^{+q}B^{+q} \leftrightarrow A^{+q-1}B^{+q+1}$, as Ref. [48] mentioned. Here, the tunneling ionization process is not taken into account while performing the computation using the over-the-barrier (OBI) model. This makes sense because there is not much time for tunneling because the pulses are so short. The outer electrons are thought to move in the double-well potential U:

$$U = -\frac{Q_1/2}{|x + R/2|} - \frac{Q_2/2}{|x - R/2|} - \varepsilon x, \tag{10}$$

where Q_1 and Q_2 represent the atomic core charges, x represents the axial position, R represents the internuclear separation, and ε is the laser E-field. The outer electron's energy level, E_L, can be approximated by

$$E_L = -\frac{(-E_1 - Q_2/R) + (-E_2 - Q_1/R)}{2}, \tag{11}$$

where E_1 and E_2 are the known ionization potentials of the atomic ions.

Figure 5 illustrates the procedure for calculating the charge transfer. The R is tiny in Figure 5a, and the center barrier is much lower than the E_L (the laser electric field introduces a considerable Stark shift, $E = \varepsilon \cdot R/2$). As a result, CT may occur effortlessly. At the intermediate R shown in Figure 5b, both the central barrier and E_L increase. Because the central barrier increases faster than E_L, the probability of CT decreases. When the probability of the charge transfer is zero, we can define the distance between the cores as R_{cr}. In Figure 5c, the R is beyond R_{cr} and the E_L is already lower than the central barrier, so that the CT process does not occur. Within the experimental conditions, the R_{cr} of each CT channel can be calculated and is labeled in Table 3.
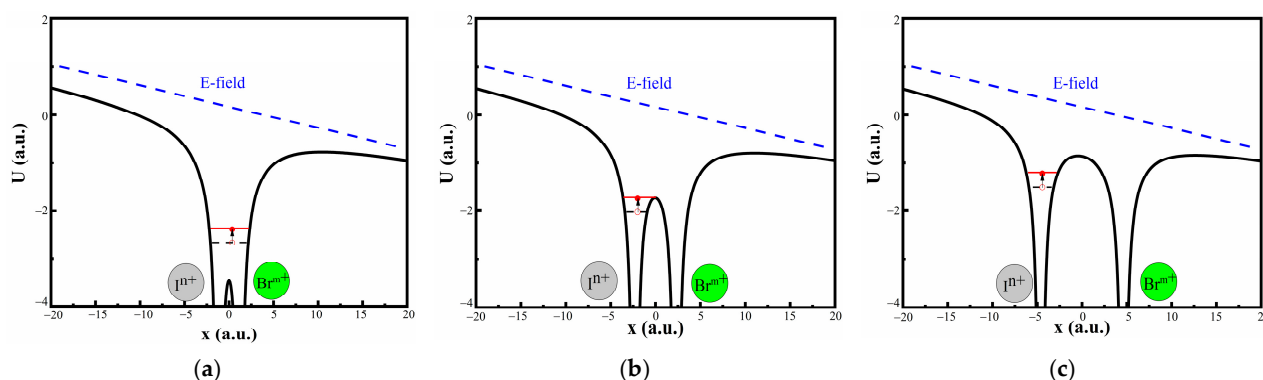
Figure 5. Double-well potential schematic diagrams for the outer electron of $IBr^{(n+m)+}$ at three internuclear separations and under a constant external electric field: (**a**) at small R, (**b**) at intermediate R, and (**c**) at long-distance R, respectively. The black dashed line represents the electron energy level E_L, while the red solid line represents the E_L with the additional Stark shift.

Table 3. Calculated R_{cr} under various laser intensities.

Channels	$R_{i,j}$ (Å)	50 TW/cm^2	100 TW/cm^2	150 TW/cm^2	200 TW/cm^2	250 TW/cm^2	300 TW/cm^2
$(1, 1) \rightarrow (1, 2) \leftrightarrow (2, 1)$	3.80	3.43	3.19	2.94	2.82	2.82	2.70
$(1, 1) \rightarrow (2, 1) \leftrightarrow (1, 2)$	4.22	3.68	3.31	3.19	3.06	2.94	2.82
$(1, 2) \rightarrow (2, 2) \leftrightarrow (3, 1)$ *	4.84	3.68	3.68	3.68	3.68	3.68	3.68
$(2, 1) \rightarrow (2, 2) \leftrightarrow (3, 1)$ *	4.55	3.68	3.68	3.68	3.68	3.68	3.68
$(2, 2) \rightarrow (3, 2) \leftrightarrow (2, 3)$	5.33	4.17	3.92	3.67	3.55	3.43	3.43
$(2, 2) \rightarrow (2, 3) \leftrightarrow (3, 2)$	4.86	3.80	3.55	3.43	3.31	3.31	3.18
$(2, 3) \rightarrow (3, 3) \leftrightarrow (4, 2)$ *	5.49	3.80	3.80	3.80	3.80	3.80	3.80

* Stark shift ($\varepsilon R/2$) is not applied to the same charged states $IBr^{(n+m)+}$ (n = m).

In Table 3, the first column represents the possible CT channels during the ionization process. The single arrow indicates the ionization process, and the double arrow represents the CT process. The second column represents the stretched value of the nuclear spacing when ionization occurs. The remaining columns indicate the R_{cr} calculated at various laser intensities. It is demonstrated that when the laser intensity rises, the R_{cr} decreases and the chance of CT rises. We are worried about whether each channel ionization and CT procedure can happen in order. Taking $(1, 1) \rightarrow (2, 1) \leftrightarrow (1, 2)$ as an example, the ionization process occurs when the internuclear distance $R_{(1,1)}$ is 4.22 Å. But for the CT process, the maximum value of R_{cr} is 3.68 Å within the experimental conditions. This means that when the stretched length of the internuclear distance exceeds 3.68 Å, the CT process is prohibited from occurring. Therefore, once the charge state (2, 1) has been formed, it has no chance to undergo further charge transfer and form the charge state (1, 2). Other channels are similar. Hence, it is not reasonable for the ionization process to occur first and then for the charge transfer process to take place.

Second, we consider the effects of the existence of the next higher process, i.e., ionization with two electrons. This is important because in the atom, the ionization rate of two electrons is usually low. However, in molecules, the ionization rate of two electrons appears to exceed the ionization rate of one electron under certain conditions. Based on the experimentally obtained channels, Table 4 considers all possible situations for the sequential ionization paths with one and two electrons. Based on the different CE channels, we also classify the above ionization paths into five categories, as shown in (f)–(j). In contrast to the one-electron sequential ionization process in Table 2, the two-electron sequential ionization process is distinguished by bolding. Taking process (f) as an example, the ionization path is $(1, 1) \rightarrow (1, 2) \rightarrow (2, 2) \rightarrow (2, 3) \rightarrow (4, 3)$. The first three steps are single ionization processes, and the last step is a double ionization process. As predicted by the "ladder-path" model, this configuration fully guarantees that the internuclear distance at the subsequent ionization phase is always higher than the internuclear distance at the preceding step. The travel

times of each ionization path are 17.55, 16.25, 7.28, and 8.59 fs, respectively. Considering that the ionization from (0, 1) to (1, 1) also takes some time, it is reasonable to expect that the entire ionization process is completed within a laser pulse of 70 fs (FMHM). At this point, we can reproduce a complete picture of all these configurations in Figure 6, where the allowed processes are shown by a solid arrow and the internuclear distance is marked when ionization takes place. With the stretching process of the molecular ions IBr^{2+} under the effect of Coulomb repulsion, enhanced ionization processes occur to form a highly charged parent ion. This observation presents more proof that ionization is predominantly controlled by states with intense coupling to the laser field. These states are strongly pushed by the laser field, leading to double ionization.

Table 4. The calculated $R_{i,j}$ and the travel time, $T_{i,j \to n,m}$, for each channel of one- and two-electron sequential ionization.

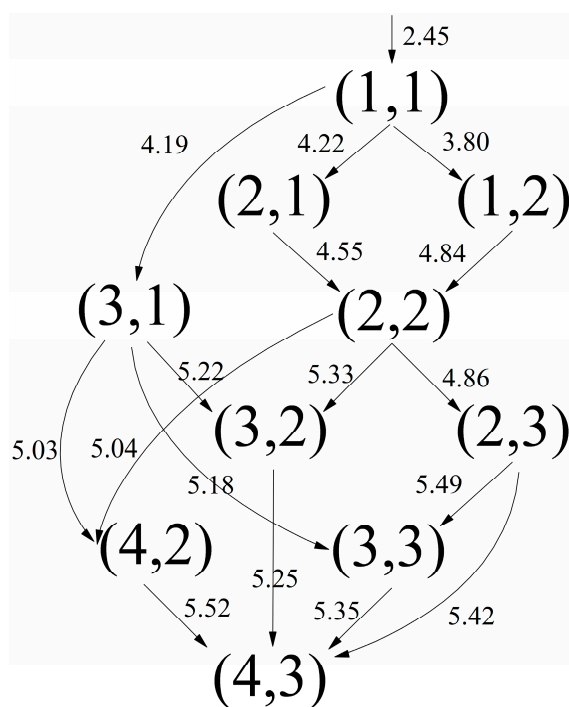| Process	Channel	$R_{i,j}$ (Å)	$T_{ij \to nm}$ (fs)
(f)	(1, 1)→(1, 2)	3.80	17.55
	(1, 2)→(2, 2)	4.84	16.25
	(2, 2)→(2, 3)	4.86	7.28
	(2, 3)→(4, 3)	5.42	8.59
(g)	(1, 1)→(1, 2)	3.80	17.55
	(1, 2)→(2, 2)	4.84	16.25
	(2, 2)→(4, 2)	5.04	9.21
	(4, 2)→(4, 3)	5.52	8.47
(h)	(1, 1)→(3, 1)	4.19	20.34
	(3, 1)→(3, 2)	5.22	14.62
	(3, 2)→(4, 3)	5.25	2.10
(i)	(1, 1)→(3, 1)	4.19	20.34
	(3, 1)→(3, 3)	5.18	14.32
	(3, 3)→(4, 3)	5.35	4.49
(j)	(1, 1)→(3, 1)	4.19	20.34
	(3, 1)→(4, 2)	5.03	13.16
	(4, 2)→(4, 3)	5.52	8.47

Figure 6. Molecular IBr's one- and two-electron ionization pathways. The values situated above the arrow signify R (Å) during ionization.

5. Conclusions

Using the DC-sliced ion velocity imaging technique, we present a collaborative experimental and theoretical investigation into the multi-electron ionization and subsequent Coulomb explosion of IBr molecules in the near-infrared femtosecond laser field. We found that the stretching of the molecular core distance could enhance the ionization to form highly charged parent ions, involving ionization with one and two electrons based on the "ladder-path" model. The results show that the higher charge states can couple strongly to the laser field. Furthermore, the charge transfer process does not occur in the experiment. This work can provide an understanding of the complex field-induced multi-electron dynamics of heteronuclear diatomic molecules.

Author Contributions: B.L. completed the experimental work and draft, and Z.L. finished part of theoretical calculation. The original experiment idea was proposed and experiments were designed by Y.Y., while Z.S. revised the manuscript and B.L. submitted the final manuscript for publication. All authors have read and agreed to the published version of the manuscript.

Institutional Review Board Statement: Not applicable.

Informed Consent Statement: Not applicable.

Data Availability Statement: Data are contained within the article.

Conflicts of Interest: The authors declare no conflict of interest.

References

1. Tang, Q.-B.; Shi, L.-K.; Zhang, K.; Kang, S.-J.; Li, Z.-F.; Wu, Y.-M.; Qin, L.-L.; Zhai, C.-Y.; Liu, A.-H.; Li, Y.-B. Electron dynamics of molecular frustrated double ionization driven by strong laser fields. *Commun. Theor. Phys.* **2023**, *75*, 035502. [CrossRef]
2. Ma, X.; Zhang, X.; Tong, A. Controlling multiple returnings in non-sequential double ionization with orthogonal two-color laser pulses. *Front. Phys.* **2023**, *11*, 1177359. [CrossRef]
3. Kang, H.; Chen, S.; Chen, J.; Paulus, G.G. Frustrated double ionization of atoms in circularly polarized laser fields. *New J. Phys.* **2021**, *23*, 033041. [CrossRef]
4. Wang, Y.; Lai, X.; Yu, S.; Sun, R.; Liu, X.; Dorner-Kirchner, M.; Erattupuzha, S.; Larimian, S.; Koch, M.; Hanus, V.; et al. Laser-Induced Electron Transfer in the Dissociative Multiple Ionization of Argon Dimers. *Phys. Rev. Lett.* **2020**, *125*, 063202. [CrossRef] [PubMed]
5. Xu, Q.-Y.; Ben, S.; Sun, Y.; Xu, H.-F.; Liu, X.-S.; Lv, H.; Guo, J. Non-sequential double ionization of triatomic molecules OCS in intense laser fields. *Chem. Phys. Lett.* **2020**, *747*, 137326. [CrossRef]
6. Li, S.; Sierra-Costa, D.; Michie, M.J.; Ben-Itzhak, I.; Dantus, M. Control of electron recollision and molecular nonsequential double ionization. *Commun. Phys.* **2020**, *3*, 35. [CrossRef]
7. Kang, H.P.; Chen, S.; Chu, W.; Yao, J.P.; Chen, J.; Liu, X.J.; Cheng, Y.; Xu, Z.Z. Nonsequential double ionization of alkaline-earth metal atoms by intense mid-infrared femtosecond pulses. *Opt. Express* **2020**, *28*, 19325–19333. [CrossRef]
8. Kang, H.; Chen, S.; Wang, Y.; Chu, W.; Yao, J.; Chen, J.; Liu, X.; Cheng, Y.; Xu, Z. Wavelength-dependent nonsequential double ionization of magnesium by intense femtosecond laser pulses. *Phys. Rev. A* **2019**, *100*, 033403. [CrossRef]
9. Cheng, C.; Vindel-Zandbergen, P.; Matsika, S.; Weinacht, T. Electron correlation in channel-resolved strong-field molecular double ionization. *Phys. Rev. A* **2019**, *100*, 053405. [CrossRef]
10. Henrichs, K.; Waitz, M.; Trinter, F.; Kim, H.; Menssen, A.; Gassert, H.; Sann, H.; Jahnke, T.; Wu, J.; Pitzer, M.; et al. Observation of Electron Energy Discretization in Strong Field Double Ionization. *Phys. Rev. Lett.* **2013**, *111*, 113003. [CrossRef]
11. Beylerian, C.; Saugout, S.E.; Cornaggia, C. Non-sequential double ionization of H_2 using ultrashort 10 fs laser pulses. *J. Phys. B At. Mol. Opt. Phys.* **2006**, *39*, L105–L112. [CrossRef]
12. Baldit, E.; Saugout, S.; Cornaggia, C. Coulomb explosion of N_2 using intense 10- and 40-fs laser pulses. *Phys. Rev. A* **2005**, *71*, 021403. [CrossRef]
13. Urbain, X.; Fabre, B.; Staicu-Casagrande, E.M.; de Ruette, N.; Andrianarijaona, V.M.; Jureta, J.; Posthumus, J.H.; Saenz, A.; Baldit, E.; Cornaggia, C. Intense-Laser-Field Ionization of Molecular Hydrogen in the Tunneling Regime and Its Effect on the Vibrational Excitation of H_2^+. *Phys. Rev. Lett.* **2004**, *92*, 163004. [CrossRef] [PubMed]
14. Cornaggia, C.; Hering, P. Nonsequential double ionization of small molecules induced by a femtosecond laser field. *Phys. Rev. A* **2000**, *62*, 023403. [CrossRef]
15. Cornaggia, C. Large-amplitude nuclear motions in the laser-induced Coulomb explosion of carbon dioxide molecules. *Phys. Rev. A* **1996**, *54*, R2555–R2558. [CrossRef] [PubMed]

16. Cornaggia, C.; Schmidt, M.; Normand, D. Laser-induced nuclear motions in the Coulomb explosion of $C_2H_2^+$ ions. *Phys. Rev. A* **1995**, *51*, 1431–1437. [CrossRef]

17. Cornaggia, C.; Lavancier, J.; Normand, D.; Morellec, J.; Liu, H.X. Intensity dependence of the multielectron dissociative ionization of N_2 at 305 and 610 nm. *Phys. Rev. A* **1990**, *42*, 5464–5472. [CrossRef]

18. Cornaggia, C.; Lavancier, J.; Normand, D.; Morellec, J.; Agostini, P.; Chambaret, J.P.; Antonetti, A. Multielectron dissociative ionization of diatomic molecules in an intense femtosecond laser field. *Phys. Rev. A* **1991**, *44*, 4499–4505. [CrossRef]

19. Keldysh, L. Ionization in the field of a strong electromagnetic wave. *Sov. Phys. JETP* **1965**, *20*, 1307–1314.

20. DeWitt, M.J.; Levis, R.J. Observing the transition from a multiphoton-dominated to a field-mediated ionization process for polyatomic molecules in intense laser fields. *Phys. Rev. Lett.* **1998**, *81*, 5101–5104. [CrossRef]

21. Hatherly, P.A.; Stankiewicz, M.; Codling, K.; Frasinski, L.J.; Cross, G.M. The multielectron dissociative ionization of molecular iodine in intense laser fields. *J. Phys. B At. Mol. Opt. Phys.* **1994**, *27*, 2993. [CrossRef]

22. Schmidt, M.; Normand, D.; Cornaggia, C. Laser-induced trapping of chlorine molecules with pico- and femtosecond pulses. *Phys. Rev. A* **1994**, *50*, 5037–5045. [CrossRef]

23. Chelkowski, S.; Bandrauk, A.D. Two-step Coulomb explosions of diatoms in intense laser fields. *J. Phys. B At. Mol. Opt. Phys.* **1995**, *28*, L723. [CrossRef]

24. Zuo, T.; Bandrauk, A.D. Charge-resonance-enhanced ionization of diatomic molecular ions by intense lasers. *Phys. Rev. A* **1995**, *52*, R2511–R2514. [CrossRef]

25. Nibarger, J.P.; Menon, S.V.; Gibson, G.N. Comprehensive analysis of strong-field ionization and dissociation of diatomic nitrogen. *Phys. Rev. A* **2001**, *63*, 053406. [CrossRef]

26. Boyer, K.; Luk, T.S.; Solem, J.C.; Rhodes, C.K. Kinetic energy distributions of ionic fragments produced by subpicosecond multiphoton ionization of N_2. *Phys. Rev. A* **1989**, *39*, 1186–1192. [CrossRef] [PubMed]

27. Gibson, G.N.; Li, M.; Guo, C.; Nibarger, J.P. Direct evidence of the generality of charge-asymmetric dissociation of molecular iodine ionized by strong laser fields. *Phys. Rev. A* **1998**, *58*, 4723–4727. [CrossRef]

28. Pavičić, D.; Kiess, A.; Hänsch, T.W.; Figger, H. Intense-Laser-Field Ionization of the Hydrogen Molecular Ions H_2^+ and D_2^+ at Critical Internuclear Distances. *Phys. Rev. Lett.* **2005**, *94*, 163002. [CrossRef] [PubMed]

29. Cornaggia, C. Electronic dynamics of charge resonance enhanced ionization probed by laser-induced alignment in C_2H_2. *J. Phys. B At. Mol. Opt. Phys.* **2016**, *49*, 19LT01. [CrossRef]

30. Cornaggia, C. Statistical analysis of fragmentation channels of small multicharged molecular ions. *J. Phys. B At. Mol. Opt. Phys.* **2012**, *45*, 085602. [CrossRef]

31. Eremina, E.; Liu, X.; Rottke, H.; Sandner, W.; Schatzel, M.G.; Dreischuh, A.; Paulus, G.G.; Walther, H.; Moshammer, R.; Ullrich, J. Influence of molecular structure on double ionization of N_2 and O_2 by high intensity ultrashort laser pulses. *Phys. Rev. Lett.* **2004**, *92*, 173001. [CrossRef]

32. Hussain, A.N.; Roberts, G. Wave packet dynamics of IBr predissociation. *J. Chem. Phys.* **1999**, *110*, 2474–2488. [CrossRef]

33. Ohmura, H.; Nakanaga, T.; Arakawa, H.; Tachiya, M. The interference effects induced by two-color excitation in the photodissociation of IBr. *Chem. Phys. Lett.* **2002**, *363*, 559–566. [CrossRef]

34. Lu, J.; Shao, F.-W.; Fan, K.-N. Coherent control of the photodissociation of CH_3I and IBr. *Chem. Phys. Lett.* **2000**, *329*, 461–468. [CrossRef]

35. Ohmura, H.; Nakanaga, T.; Tachiya, M. Coherent control of photofragment separation in the dissociative ionization of IBr. *Phys. Rev. Lett.* **2004**, *92*, 113002. [CrossRef]

36. Zhang, J.; Li, Z.; Yang, Y. Multi-ionization of the Cl_2 molecule in the near-infrared femtosecond laser field. *RSC Adv.* **2020**, *10*, 332–337. [CrossRef] [PubMed]

37. Zhang, J.; Yang, Y.; Li, Z.; Sun, H.; Zhang, S.; Sun, Z. Channel-resolved multiorbital double ionization of molecular Cl_2 in an intense femtosecond laser field. *Phys. Rev. A* **2018**, *98*, 043402. [CrossRef]

38. Guo, C.L.; Li, M.; Gibson, G.N. Charge asymmetric dissociation induced by sequential and nonsequential strong field ionization. *Phys. Rev. Lett.* **1999**, *82*, 2492–2495. [CrossRef]

39. Frisch, M.J.; Trucks, G.W.; Schlegel, H.B.; Scuseria, G.E.; Robb, M.A.; Cheeseman, J.R.; Scalmani, G.; Barone, V.; Mennucci, B.; Petersson, G.A.; et al. *Gaussian 09, Revision D. 01*; Gaussian Inc.: Wallingford, UK, 2009.

40. Lee, C.; Yang, W.; Parr, R.G. Development of the Colle-Salvetti correlation-energy formula into a functional of the electron density. *Phys. Rev. B* **1988**, *37*, 785. [CrossRef]

41. Woon, D.E.; Dunning, T.H., Jr. Gaussian basis sets for use in correlated molecular calculations. III. The atoms aluminum through argon. *J. Chem. Phys.* **1993**, *98*, 1358–1371. [CrossRef]

42. Stanton, J.F.; Bartlett, R.J. The equation of motion coupled-cluster method. A systematic biorthogonal approach to molecular excitation energies, transition probabilities, and excited state properties. *J. Chem. Phys.* **1993**, *98*, 7029–7039. [CrossRef]

43. Kállay, M.; Gauss, J. Calculation of excited-state properties using general coupled-cluster and configuration-interaction models. *J. Chem. Phys.* **2004**, *121*, 9257–9269. [CrossRef]

44. Yang, Y.; Fan, L.; Sun, S.; Zhang, J.; Chen, Y.; Zhang, S.; Jia, T.; Sun, Z. Dissociative double ionization of 1-bromo-2-chloroethane irradiated by an intense femtosecond laser field. *J. Chem. Phys.* **2011**, *135*, 064303. [CrossRef] [PubMed]

45. Wu, C.; Yang, Y.; Wu, Z.; Chen, B.; Dong, H.; Liu, X.; Deng, Y.; Liu, H.; Liu, Y.; Gong, Q. Coulomb explosion of nitrogen and oxygen molecules through non-Coulombic states. *Phys. Chem. Chem. Phys.* **2011**, *13*, 18398. [CrossRef] [PubMed]

46. Walker, B.; Sheehy, B.; DiMauro, L.F.; Agostini, P.; Schafer, K.J.; Kulander, K.C. Precision Measurement of Strong Field Double Ionization of Helium. *Phys. Rev. Lett.* **1994**, *73*, 1227–1230. [CrossRef] [PubMed]

47. Menon, S.; Nibarger, J.P.; Gibson, G.N. A framework for understanding molecular ionization in strong laser fields. *J. Phys. B At. Mol. Opt. Phys.* **2002**, *35*, 2961–2974. [CrossRef]

48. Kawata, I.; Kono, H.; Fujimura, Y.; Bandrauk, A.D. Intense-laser-field-enhanced ionization of two-electron molecules: Role of ionic states as doorway states. *Phys. Rev. A* **2000**, *62*, 031401. [CrossRef]